

Comparison of the Association Level of a Pyrene-Labeled Associative Polymer Obtained from an Analysis Based on Two Different Models

Howard Siu and Jean Duhamel*

Institute for Polymer Research, Department of Chemistry, University of Waterloo, Waterloo, ON N2L 3G1, Canada

Received: September 19, 2004; In Final Form: November 8, 2004

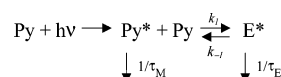
A hydrophobically modified alkali swellable emulsion copolymer (HASE) was labeled with pyrene and its fluorescence behavior was monitored by steady-state and time-resolved fluorescence as increasing amounts of the surfactant sodium dodecyl sulfate (SDS) were added to the solution. In aqueous solution, the pyrene pendants are aggregated. As SDS is added, the surfactant binds to the pyrene aggregates, which leads to their breakup at an onset SDS concentration of 1.25×10^{-3} mol/L. The breakup of the pyrene aggregates is complete at 4.25×10^{-3} mol/L, which is slightly larger than the critical micellar concentration of SDS in 0.01 M Na_2CO_3 aqueous solution at pH 9 found to equal 3.5×10^{-3} mol/L by surface tension measurements. The pyrene pendants were present as different species in solution, and the fractions representative of all emissive pyrene species were determined from the global analysis of the monomer and excimer fluorescence decays. Two analyses were applied to the decays. In the first analysis, the diffusional encounters between pyrene pendants were described by the blob model. In the second analysis, no assumptions were made on how the pyrene pendants encountered each other. Both analyses yielded identical results which demonstrate that the determination of the fractions of the different emissive pyrene species of a solution of a pyrene-labeled associative polymer does not depend on the model chosen to account for the diffusional encounters taking place between pyrene pendants.

Introduction

Water-soluble associative polymers (APs) are water-soluble polymers onto which hydrophobic compounds have been attached. Although such polymers remain soluble in water, the hydrophobes induce the formation of intra- (at low polymer concentration) or intermolecular (at high polymer concentration) hydrophobic aggregates. Extensive intermolecular aggregation leads to the formation of a polymer network, which is accompanied by a drastic increase in the solution viscosity. Because the polymeric aggregates are held together by physical interactions between the hydrophobes, they can be broken up under shear, resulting in a drastic drop in viscosity. These peculiar viscoelastic properties of APs have led to numerous applications in industry settings¹ and have generated a strong academic interest.² The chemical structure³ and geometry⁴ of the hydrophobes has been shown to play an important role in controlling the viscoelastic properties of an AP in solution and techniques capable of probing the behavior of an AP's hydrophobes in solution are of tremendous use to better understand how APs work.

Over the years, fluorescence has established itself as a powerful technique to study polymeric systems.⁵ One particular application to the study of APs by fluorescence involves the labeling of a water-soluble polymer with the hydrophobic probe pyrene.⁶ Such pyrene-labeled polymers have behaviors which mimic that of APs and the fluorescence response of pyrene can be used to infer how the hydrophobes behave in solution.⁷ These pyrene-labeled APs will be referred to as Py-APs. Because an excited pyrene monomer, emitting in the blue region, can form an excited complex called an excimer, which emits in the green region, the extent of excimer formation determined as the ratio

SCHEME 1



of excimer fluorescence intensity over monomer fluorescence intensity (or the I_E/I_M ratio) provides some information about the level of association of the hydrophobic pendants of a Py-AP.⁷ This is of particular interest to the study of APs since the viscoelastic properties of their solution depend on the level of associations of an AP's hydrophobes.⁸ Work from this laboratory has demonstrated that the fraction of aggregated pyrenes (f_{agg}) can be determined quantitatively by using the ability of pyrene to form an excimer.^{9–13}

In the case of a solution of molecular pyrene (cf. Scheme 1), the excited pyrene can either fluoresce with its own lifetime, τ_M , or encounter a ground-state pyrene to form an excited complex called an excimer, which fluoresces with its own lifetime, τ_E . The rate constant of excimer formation, k_1 , the dissociation rate constant, k_{-1} , and τ_E can be determined from a Birks' scheme analysis of the monomer and excimer fluorescence decays.¹⁴ Under these conditions, there is a single rate constant for excimer formation and no pyrene aggregates are present in solution. Solutions of randomly labeled Py-APs present a much more complicated situation for two main reasons. First, the rate of excimer formation depends strongly on the chain length spanning¹⁵ and flanking¹⁶ two pyrene labels. Since the probes are incorporated randomly into the polymer backbone, there is a distribution of chain lengths spanning and flanking two pyrenes, and a distribution of rate constants for excimer formation.¹⁷ This distribution of rate constants greatly complicates the quantitative analysis of the decays obtained with

polymers randomly labeled with pyrene. Second, excimers of a Py-AP in water are formed not only by the diffusional encounter between an excited pyrene and a ground-state pyrene, but also from the direct excitation of pyrene aggregates. This is another feature absent from Scheme 1.

To deal with the distribution of rate constants for excimer formation, a model was developed, called the blob model, whereby a blob is defined as the volume probed by an excited pyrene during its lifetime.¹⁸ The blob model has been shown to be a powerful tool to study polymer chain dynamics,^{18,19} the volume probed by the side chain of an α -helical poly(L-glutamic acid),¹¹ or more recently, coil-to-globule transitions.^{20,21} In the case of Py-APs solutions, the blob model has been used to account for the diffusional encounters occurring between an excited pyrene and a ground-state pyrene, either isolated or located inside a pyrene aggregate.^{9,10,12,13} It was shown that the fraction of aggregated pyrene pendants (f_{agg}) can be determined by combining the results obtained by fitting the pyrene monomer and excimer decays. This procedure was applied to determine the level of association of several pyrene-labeled polymers including a series of hydrophobically modified alkali swellable emulsion polymers (HASE)⁹ and poly(*N,N*-dimethyl acrylamide)s,¹⁰ poly(L-glutamic acid),¹¹ maleated ethylene-propylene random copolymer,¹² and polystyrene.²¹ More recently, the level of pyrene association of a pyrene-labeled HASE was determined as increasing amounts of the surfactant sodium dodecyl sulfate (SDS) were added to the solution.¹³ As the surfactant binds to the pyrene aggregates, the level of aggregation is found to drop precipitously in the neighborhood of the surfactant critical micellar concentration (CMC) for a polymer concentration of 1 g/L.

The blob model has been very helpful in determining f_{agg} by providing a mathematical tool that describes the diffusional encounters occurring between pyrene pendants. The expression of the "time-dependent rate constant" of excimer formation for a polymer randomly labeled with pyrene can be determined exactly with the blob model and is referred to as $f(t)$. Yet the use of the blob model to determine the function $f(t)$ is not mandatory. As will be shown in the present study, the function $f(t)$ describing the diffusional encounters between pyrenes can also be approximated by a sum of exponentials. As it turns out, such an approximation allows one to fit the monomer and excimer decays with sums of exponentials. This proposed mathematical treatment is expected to find numerous applications since many studies performed on pyrene-labeled polymers use sums of exponentials^{22–24} to fit the fluorescence decays rather than the more intricate blob model.^{9–13,18–21}

To provide an experimental support to these mathematical considerations, the monomer and excimer fluorescence decays were acquired for a solution of a pyrene-labeled HASE (Py-HASE) to which increasing amounts of the SDS surfactant were added. In basic aqueous solution, the pyrene pendants of Py-HASE are aggregated. Addition of surfactant to the solution generates hydrophobic microdomains which dissolve the pyrene aggregates. Consequently the level of pyrene aggregation undergoes drastic changes upon addition of SDS. This polymer/surfactant combination provides an ideal experimental system to investigate how different analyses perform in retrieving the f_{agg} parameter.

The kinetics of monomer consumption and excimer formation are coupled when the excimer is formed by diffusion.¹⁴ As a result, several decay times are often found to be the same in the monomer and excimer decays when they are fitted with sums of exponentials. The ultimate analysis procedure fits the

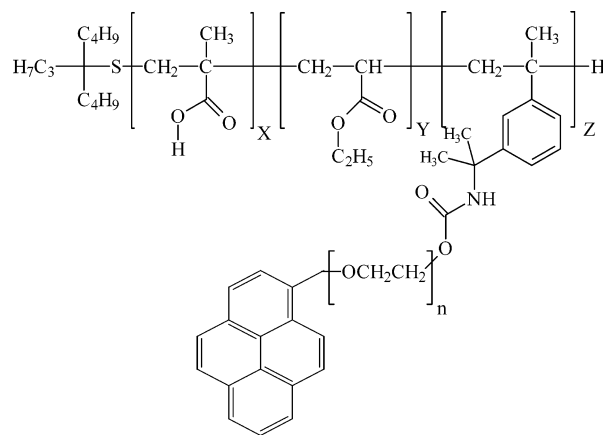


Figure 1. Chemical structure of Py-HASE with $X = 0.45$, $Y = 0.54$, $Z = 0.01$, $n = 53$.

monomer and excimer fluorescence decays globally by ensuring that some of the decay times are held the same in both the monomer and excimer decays. Global analysis ensures that the parameters from the analysis of the fluorescence decays are retrieved with higher accuracy.²⁵ The monomer and excimer fluorescence decays of a Py-HASE were fitted globally by using two procedures depending on whether the function $f(t)$ was determined exactly with the blob model or approximated by a sum of exponentials. The parameters retrieved from both analyses were compared to assess whether an analysis based on sums of exponentials yields results which agree with those obtained with a blob model-based analysis.

The structure of the Py-HASE polymer used in this study is shown in Figure 1. It is a terpolymer made of methacrylic acid, ethyl acrylate, and a small amount of hydrophobically modified macromonomer (HMM). HMM is a poly(ethylene oxide) (PEO) spacer terminated at one end with a hydrophobe, a pyrene group in the case of Py-HASE.² The other end of the PEO spacer is connected to a methylstyrene monomer via a urethane linker. Basic conditions ionize the polymeric backbone, which expands in solution due to electrostatic repulsions. Microcalorimetry experiments have shown that SDS binds onto a HASE polymer where the HMM is terminated by a methyl group, which demonstrates that the presence of hydrophobes is not necessary for SDS to bind to HASE.²⁶ Yet binding is substantially enhanced when HASE is hydrophobically modified with long alkyl chains (C16, C20).²⁶ SDS binding onto HASE has also been shown to depend on the PEO spacer length.²⁷ The long PEO spacer (53 ethylene oxide units for Py-HASE) is expected to provide enough flexibility for the formation of large hydrophobic aggregates which are more accessible to surfactant molecules than the hydrophobic aggregates of HASEs that have a PEO spacer made of less than 10 ethylene oxide units.²⁷ To date, most of the information acquired on HASEs has been obtained with HASEs bearing alkyl chains as the hydrophobes. Experiments carried out with Py-HASE allow information to be gained on the specific behavior of the hydrophobes (the fluorescent pyrene pendants).

Theory

Traditionally the determination of the f_{agg} parameter for a Py-AP, a measure of the level of pyrene aggregation, has been carried out by analyzing the fluorescence decays of the monomer and the excimer with use of a blob model.^{9–13,21} The presence of four emissive pyrene species is assumed in the analysis. The first one is $\text{Py}_{\text{diff}}^*$, which represents those pyrenes which form

the excimer, $E0^*$, via diffusion with a “time-dependent rate constant” $f(t)$. The second species is constituted by those pyrenes which are too isolated to form excimer and fluoresce with their lifetime τ_M , Py_{free}^* . The third and fourth ones represent the preassociated pyrenes which upon absorption of a photon exhibit the proper stacking to form the excimer $E0^*$ and an improper stacking resulting in the formation of long-lived excimer, D^* , respectively. The lifetimes of $E0^*$ and D^* are referred to as τ_{E0} and τ_D , respectively. Four differential equations are necessary to describe the time-dependent profiles of these four pyrene species. They are given hereafter with the corresponding initial conditions.

$$\frac{d[Py_{diff}^*]}{dt} = -\frac{1}{\tau_M}[Py_{diff}^*] - f(t) \text{ where } [Py_{diff}^*]_{(t=0)} = [Py_{diff}^*]_0 \quad (1)$$

$$\frac{d[Py_{free}^*]}{dt} = -\frac{1}{\tau_M}[Py_{free}^*] \text{ where } [Py_{free}^*]_{(t=0)} = [Py_{free}^*]_0 \quad (2)$$

$$\frac{d[E0^*]}{dt} = -\frac{1}{\tau_{E0}}[E0^*] + f(t) \text{ where } [E0^*]_{(t=0)} = [E0^*]_0 \quad (3)$$

$$\frac{d[D^*]}{dt} = -\frac{1}{\tau_D}[D^*] \text{ where } [D^*]_{(t=0)} = [D^*]_0 \quad (4)$$

These equations assume that the dissociation of the pyrene excimer is negligible at room temperature, as is often found in the literature.²⁰ The function $f(t)$ used in eq 1 arises from the inhomogeneous distribution of pyrene groups inside the polymer coil. Due to the random incorporation of pyrenes, some domains in the polymer coil are pyrene-rich whereas other domains are pyrene-poor. Consequently those pyrene-rich domains form excimer on a fast time scale with a large rate constant whereas those pyrene-poor domains form excimer on a slow time scale with a small rate constant. As a result, the rate constant of excimer formation by diffusion is expected to decrease over time and it is given by the time-dependent function, $f(t)$.

Equations 1–4 are linear first-order equations. They can be solved easily so that the time-dependent concentration of pyrene monomer and excimer can be expressed as the sums $[Py^*]_{(t)} = [Py_{diff}^*]_{(t)} + [Py_{free}^*]_{(t)}$ and $[E^*]_{(t)} = [E0^*]_{(t)} + [D^*]_{(t)}$, respectively. The expressions of $[Py^*]_{(t)}$ and $[E^*]_{(t)}$ are given in eqs 5 and 6.

$$[Py^*]_{(t)} = \exp(-t/\tau_M)[[Py_{diff}^*]_{(t=0)} - \int_{u=0}^t f(u) \exp(u/\tau_M) du] + [Py_{free}^*]_{(t=0)} \exp(-t/\tau_M) \quad (5)$$

$$[E^*]_{(t)} = \exp(-t/\tau_{E0})[[E0^*]_{(t=0)} + \int_{u=0}^t f(u) \exp(u/\tau_{E0}) du] + [D^*]_{(t=0)} \exp(-t/\tau_D) \quad (6)$$

The first term in eq 5 represents the time-dependent profile $[Py_{diff}^*]_{(t)}$. The key step in solving eqs 5 and 6 is the determination of $f(t)$ from eq 1. This is done by assuming a function for $[Py_{diff}^*]_{(t)}$, solving for $f(t)$ in eq 1, and using the expression of $f(t)$ to solve eqs 5 and 6. Traditionally this laboratory has used the blob model expression to provide a mathematical expression of $[Py_{diff}^*]_{(t)}$ as shown in the first term of eq 7.^{9–13,18–21}

$$[Py^*]_{(t)} = [Py_{diff}^*]_{(t=0)} \exp\left(-\left(A_2 + \frac{1}{\tau_M}\right)t - A_3(1 - \exp(-A_4 t)) + [Py_{free}^*]_{(t=0)} \exp(-t/\tau_M) \quad (7)$$

where the coefficients A_2 , A_3 , and A_4 are given hereafter.

$$A_2 = \langle n \rangle \frac{k_{blob} k_e [blob]}{k_{blob} + k_e [blob]}; A_3 = \langle n \rangle \frac{k_{blob}^2}{(k_{blob} + k_e [blob])^2}; A_4 = k_{blob} + k_e [blob] \quad (8)$$

The coefficients A_2 , A_3 , and A_4 are functions of the average number of pyrene groups in a blob, $\langle n \rangle$, the rate constant of excimer formation inside a blob, k_{blob} , between one excited and one ground-state pyrene, and the rate at which pyrene groups exchange from blob to blob, $k_e [blob]$, where k_e is the exchange rate constant and $[blob]$ is the blob concentration inside the polymer coil. The stretched exponential given in eq 7 can be developed into an infinite series of exponentials that is used in eq 1 to obtain $f(t)$, which is itself a series of exponentials. A series of exponentials being easily integrated, the following expression is obtained for $[E^*]$.

$$[E^*] = -[Py_{diff}^*]_{(t=0)} e^{-A_3} \sum_{i=0}^{\infty} \frac{A_3^i}{i!} \frac{A_2 + iA_4}{\frac{1}{\tau_M} - \frac{1}{\tau_{E0}} + A_2 + iA_4} \times \exp\left(-\left(\frac{1}{\tau_M} + A_2 + iA_4\right)t\right) + \left([E0^*]_{(t=0)} + [Py_{diff}^*]_{(t=0)} e^{-A_3} \sum_{i=0}^{\infty} \frac{A_3^i}{i!} \frac{A_2 + iA_4}{\frac{1}{\tau_M} - \frac{1}{\tau_{E0}} + A_2 + iA_4}\right) e^{-t/\tau_{E0}} + [D^*]_{(t=0)} e^{-t/\tau_D} \quad (9)$$

To relate eqs 7 and 9 to fluorescence decays obtained by time-resolved fluorescence, the concentrations of the various fluorescing species must be weighed by their extinction coefficients and radiative rate constants. To do so, eqs 7 and 9 are rewritten into the easier to handle expressions given in eqs 10 and 11.

$$[Py^*] = [Py_{diff}^*]_{(t=0)} G_M(t) + [Py_{free}^*]_{(t=0)} \exp(-t/\tau_M) \quad (10)$$

$$[E^*] = -[Py_{diff}^*]_{(t=0)} G_E(t) + ([E0^*]_{(t=0)} + [Py_{diff}^*]_{(t=0)} G_E(t=0)) e^{-t/\tau_{E0}} + [D^*]_{(t=0)} e^{-t/\tau_D} \quad (11)$$

The expressions of $G_M(t)$ and $G_E(t)$ can be easily obtained by comparing eqs 10 and 11 with eqs 7 and 9, respectively. They are given in Table 1 in the Supporting Information. Equations 10 and 11 can be used to obtain the time dependence of the monomer and excimer fluorescence intensities given in eqs 12 and 13:

$$I_M(t) = \alpha(\lambda_{ex}, \lambda_{em}) \{ \epsilon_M k_{rad}^M [Py_{diff}^*]_{(t=0)} G_M(t) + \epsilon_M k_{rad}^M [Py_{free}^*]_{(t=0)} \exp(-t/\tau_M) \} \quad (12)$$

$$I_E(t) = \alpha(\lambda_{ex}, \lambda_{em}) \{ -\epsilon_M k_{rad}^{E0(diff)} [Py_{diff}^*]_{(t=0)} G_E(t) + (\epsilon_{E0} k_{rad}^{E0(agg)} [E0^*]_{(t=0)} + \epsilon_M k_{rad}^{E0(diff)} [Py_{diff}^*]_{(t=0)} \times G_E(t=0)) e^{-t/\tau_{E0}} + \epsilon_D k_{rad}^D [D^*]_{(t=0)} e^{-t/\tau_D} \} \quad (13)$$

In eqs 12 and 13, the extinction coefficients and radiative rate

constants are referred to as ϵ_X and k_{rad}^X , respectively, where the index X stands for either the pyrene monomer ($M = \text{Py}_{\text{diff}}$ or Py_{free}) or the pyrene excimer and dimer ($E0$ or D). Whether the pyrene excimer is formed by diffusion or direct excitation is indicated as $E0^*(\text{diff})$ or $E0^*(\text{agg})$, respectively. The coefficient $\alpha(\lambda_{\text{ex}}, \lambda_{\text{em}})$ is a parameter that depends on the excitation and emission wavelengths as well as the geometry of the time-resolved fluorometer.

In the global analysis of the monomer and excimer decays, the parameters A_2 , A_3 , and A_4 used in the functions $G_M(t)$ and $G_E(t)$ are kept the same. When eqs 12 and 13 are used to fit the monomer and excimer decays, respectively, the preexponential factors retrieved from the analysis yield the fractions of the fluorescence intensity emitted by each emissive pyrene species present in solution. The expressions of those fractions are given in eqs 14–17. It is clear from eqs 14–17 that if one assumes that $\epsilon_M = \epsilon_{E0} = \epsilon_D$ and $k_{\text{rad}}^{E0(\text{diff})} = k_{\text{rad}}^{E0(\text{agg})} = k_{\text{rad}}^D$, the fractions f_{diff} , f_{free} , f_{E0} , and f_D are equivalent to the molar fractions of all emissive pyrene species present in solution and the sum $f_{\text{agg}} = f_{E0} + f_D$ is the fraction of all aggregated pyrenes. As can be seen in the Appendix, this equivalence is expected to hold when the pyrene pendants are strongly or weakly aggregated. At the transition where a pyrene-labeled polymer switches from a state where the pyrenes are strongly aggregated to a state where the pyrenes are weakly aggregated, the fractions f_{diff} , f_{free} , f_{E0} , and f_D reflect the occurrence of the transition but provide only qualitative information about the behavior of the fractions of the corresponding emissive pyrene species.

$$f_{\text{diff}} = \frac{[\text{Py}_{\text{diff}}^*]_{(t=0)}}{[\text{Py}_{\text{diff}}^*]_{(t=0)} + [\text{Py}_{\text{free}}^*]_{(t=0)} + \frac{\epsilon_{E0} k_{\text{rad}}^{E0(\text{agg})}}{\epsilon_M k_{\text{rad}}^{E0(\text{diff})}} [\text{E0}^*]_{(t=0)} + \frac{\epsilon_D k_{\text{rad}}^D}{\epsilon_M k_{\text{rad}}^{E0(\text{diff})}} [\text{D}^*]_{(t=0)}} \quad (14)$$

$$f_{\text{free}} = \frac{[\text{Py}_{\text{free}}^*]_{(t=0)}}{[\text{Py}_{\text{diff}}^*]_{(t=0)} + [\text{Py}_{\text{free}}^*]_{(t=0)} + \frac{\epsilon_{E0} k_{\text{rad}}^{E0(\text{agg})}}{\epsilon_M k_{\text{rad}}^{E0(\text{diff})}} [\text{E0}^*]_{(t=0)} + \frac{\epsilon_D k_{\text{rad}}^D}{\epsilon_M k_{\text{rad}}^{E0(\text{diff})}} [\text{D}^*]_{(t=0)}} \quad (15)$$

$$f_{E0} = \frac{\frac{\epsilon_{E0} k_{\text{rad}}^{E0(\text{agg})}}{\epsilon_M k_{\text{rad}}^{E0(\text{diff})}} [\text{E0}^*]_{(t=0)}}{[\text{Py}_{\text{diff}}^*]_{(t=0)} + [\text{Py}_{\text{free}}^*]_{(t=0)} + \frac{\epsilon_{E0} k_{\text{rad}}^{E0(\text{agg})}}{\epsilon_M k_{\text{rad}}^{E0(\text{diff})}} [\text{E0}^*]_{(t=0)} + \frac{\epsilon_D k_{\text{rad}}^D}{\epsilon_M k_{\text{rad}}^{E0(\text{diff})}} [\text{D}^*]_{(t=0)}} \quad (16)$$

$$f_D = \frac{\frac{\epsilon_D k_{\text{rad}}^D}{\epsilon_M k_{\text{rad}}^{E0(\text{diff})}} [\text{D}^*]_{(t=0)}}{[\text{Py}_{\text{diff}}^*]_{(t=0)} + [\text{Py}_{\text{free}}^*]_{(t=0)} + \frac{\epsilon_{E0} k_{\text{rad}}^{E0(\text{agg})}}{\epsilon_M k_{\text{rad}}^{E0(\text{diff})}} [\text{E0}^*]_{(t=0)} + \frac{\epsilon_D k_{\text{rad}}^D}{\epsilon_M k_{\text{rad}}^{E0(\text{diff})}} [\text{D}^*]_{(t=0)}} \quad (17)$$

As for any other technique, fluorescence tracks the behavior of only those pyrene species which fluoresce. Consequently, any nonemissive pyrene species present in solution is not accounted for by a fluorescence experiment. The existence of nonemissive pyrene aggregates has been suggested in several

publications.^{24,28,29} Such species jeopardize the equivalence that exists between f_{diff} , f_{free} , f_{E0} , and f_D and the molar fractions of all pyrene species present in solution under conditions where the pyrene pendants are strongly or weakly associated. However, the weak emission reported for pyrene aggregates^{24,28,29} could also result from a low $k_{\text{rad}}^{E0(\text{agg})}$ value, i.e., the pyrene aggregates are poor emitters which can be detected by a fluorescence experiment rather than nonemitters ($k_{\text{rad}}^{E0(\text{agg})} = 0 \text{ s}^{-1}$). In any case, the results of the fluorescence experiments presented in this work will report on all the emissive pyrene species, bearing in mind that not all pyrene species present in solution might fluoresce.

The procedure outlined above has been very successful at determining the parameter $f_{\text{agg}} = f_{E0} + f_D$ for a number of pyrene-labeled polymers.^{9–13,21} Yet the determination of f_{agg} is not expected to depend on the model chosen to handle the diffusional encounters between pyrene pendants, i.e., the blob model. To verify this point, the analysis procedure was redesigned in a way that would avoid any use of the blob model. To do so, $[\text{Py}_{\text{diff}}^*]_{(t)}$ was approximated by a sum of exponentials, so that eq 18 can be applied instead of using eq 7.

$$[\text{Py}^*]_{(t)} = [\text{Py}_{\text{diff}}^*]_{(t=0)} \sum_{i=1}^n a_i e^{-t/\tau_i} + [\text{Py}_{\text{free}}^*]_{(t=0)} \exp(-t/\tau_M) \quad (18)$$

The expression of $[\text{Py}_{\text{diff}}^*]_{(t)}$ being a sum of exponentials, the function $f(t)$ can be easily determined from eq 1 and can be used to find the time-dependent profile of $[E^*]_{(t)}$ from eq 6. It is given in eq 19.

$$[\text{E0}^*] = -[\text{Py}_{\text{diff}}^*]_{(t=0)} \sum_{i=0}^{\infty} a_i \frac{\frac{1}{\tau_i} - \frac{1}{\tau_{E0}}}{\frac{1}{\tau_i} - \frac{1}{\tau_M}} e^{-t/\tau_i} + \left([\text{E0}^*]_{(t=0)} + [\text{Py}_{\text{diff}}^*]_{(t=0)} \sum_{i=0}^{\infty} a_i \frac{\frac{1}{\tau_i} - \frac{1}{\tau_{E0}}}{\frac{1}{\tau_i} - \frac{1}{\tau_M}} \right) e^{-t/\tau_{E0}} + [\text{D}^*]_{(t=0)} e^{-t/\tau_D} \quad (19)$$

Equations 18 and 19 are used to describe the time-dependent profiles of the pyrene monomer and excimer. They adopt expressions similar to those of eqs 10 and 11. The expressions of the functions $G_M(t)$ and $G_E(t)$ can be found by comparing eqs 10 and 18 and eqs 11 and 19, respectively. They are given in Table 1 in the Supporting Information. Consequently eqs 12 and 13 can be applied to fit the monomer and excimer decays according to the expressions of $G_M(t)$ and $G_E(t)$ inferred from eqs 18 and 19. The analysis of the monomer and excimer decays with eqs 12 and 13 is performed globally by maintaining the lifetimes τ_i the same in the expressions of $G_M(t)$ and $G_E(t)$. The fractions f_{diff} , f_{free} , f_{E0} , and f_D are determined by using eqs 14–17. By using a sum of exponentials to fit the monomer decays, no assumption is being made on how to model the encounters between pyrene pendants.

Experimental Section

All chemicals and instrumentation used in this study have been described in an earlier publication.⁹ The Py-HASE had a pyrene content of 36 μmol of pyrene per gram of polymer. Its chemical structure is given in Figure 1. All experiments were performed under basic conditions in aqueous solution (0.01 M

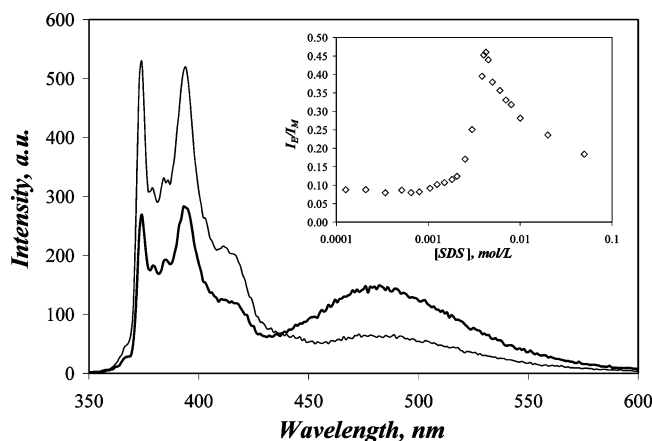


Figure 2. Fluorescence spectra of Py-HASE in water (light line) and in 4.25×10^{-3} mol/L SDS (heavy line) in 0.01 M Na_2CO_3 aqueous solution at pH 9 ($\lambda_{\text{ex}} = 344$ nm). The inset shows the I_E/I_M ratio as a function of SDS concentration.

Na_2CO_3 , pH 9). The only differences with the earlier work dealt with the instrument used to acquire the fluorescence decays and the use of a DuNouy tensiometer for surface tension measurements.

Time-Resolved Fluorescence Decays. Fluorescence decays were acquired by the Time-Correlated Single Photon Counting (TCSPC) technique with an IBH time-resolved fluorometer, using 1024 channels for both the pyrene monomer and excimer decays. For all samples, the excitation wavelength was 344 nm, and the fluorescence from the pyrene monomer and excimer was monitored at 374 and 510 nm, respectively. To block potential light scattering leaking through the detection system, filters were used with a cutoff at 370 and 495 nm to acquire the fluorescence decays of the pyrene monomer and excimer, respectively. A minimum of 40 000 and 10 000 counts was collected at the maximum of the fluorescence decays of the pyrene monomer and excimer, respectively. The analyses of the decay curves were performed with the δ -pulse deconvolution. Reference decay curves of degassed solutions of PPO [2,5-diphenyloxazole] in cyclohexane ($\tau = 1.42$ ns) and BBOT [2,5-bis(5-*tert*-butyl-2-benzoxazolyl) thiophene] in ethanol ($\tau = 1.47$ ns) were used for the analyses of the monomer and excimer decay curves, respectively.

Surface Tension Measurements. All surface tension measurements were done on a DuNouy ring tensiometer. The ring was initially prepared for measurement by lightly flaming it to remove any organic particles clinging to the ring. Afterward, the ring was cleaned by washing with a soap and water solution and then rinsing with milli-Q water and methanol and then dried with compressed nitrogen gas. The glass sample vessel was similarly cleaned with soap, water, and methanol and dried with nitrogen gas. The samples were placed into the glass vessel and the ring was immersed into the solution. The surface tension was measured. The value was then recorded as the measured surface tension and was corrected by multiplying by a correction factor obtained from a chart supplied by the manufacturer (Central Scientific Company, Inc.). The sample was removed from the vessel and both the ring and the vessel were cleaned as described above before the next measurement.

Results and Discussion

Addition of SDS to a solution of pyrene-labeled HASE did affect the features of the fluorescence spectrum, as illustrated in Figure 2. At low SDS concentration, little excimer is being

formed (cf. light trace in Figure 2). Although this low level of excimer formation was believed to arise from the coil expansion of Py-HASE due to the negative charges distributed along the polymer backbone,⁹ it could also be due to the low fluorescence quantum yield of pyrene aggregates.^{24,28,29} As will be confirmed later by time-resolved fluorescence measurements, very few excimers are formed by diffusional encounters between pyrene pendants at low SDS concentration and most of the excimer fluorescence arises from direct excitation of ground-state pyrene aggregates. Yet the ratio of the excimer fluorescence intensity over that of the monomer, the I_E/I_M ratio, is low in aqueous solution and equals 0.09. At low SDS concentration, the pyrene monomer is either exposed to water or wrapped inside the PEO spacer of the HASE macromonomer and the ratio of the intensities of the first peak over that of the third peak, the I_1/I_3 ratio, equals 1.60 ± 0.02 . This value is comparable to that obtained for a poly(ethylene oxide) chain labeled at one end with pyrene (Py-PEO) in the same SDS concentration range (1.69 ± 0.03). Addition of SDS to the Py-HASE solution melts the pyrene aggregates in a process that pulls the pyrene pendants into the SDS micelles. For SDS concentrations close to the CMC measured by surface tension to equal 3.5×10^{-3} mol/L for SDS in 0.01 M Na_2CO_3 aqueous solution at pH 9 (cf. Supporting Information), the pyrene pendants are concentrated inside a few SDS micelles, the formation of excimer is favored, and the I_E/I_M ratio is large (cf. thick trace in Figure 2). At its maximum value, the I_E/I_M ratio equals 0.46 for an SDS concentration of 4.25×10^{-3} mol/L (cf. inset in Figure 2) representing a 5-fold increase when compared to the I_E/I_M ratio in aqueous solution. The pyrene pendants experience the more hydrophobic environment of the SDS micelles as indicated by an I_1/I_3 value of 1.31 ± 0.04 . Here again this value is similar to that of the Py-PEO model compound at high SDS concentration (1.38 ± 0.02) when the pyrene moiety interacts with the hydrophobic interior of the SDS micelles. At this SDS concentration, a majority of pyrene pendants form excimer via diffusion, which will be confirmed by the analysis of the fluorescence decays. For SDS concentrations larger than 4.25×10^{-3} mol/L, more SDS micelles are formed, the pyrene pendants distribute themselves randomly among an increasing number of SDS micelles, and the I_E/I_M ratio decreases (cf. inset in Figure 2).

The interactions between different pyrene-labeled polymers and SDS have been reported by several other research groups.^{28–31} In all cases, the studies revolved mainly around the behavior of the I_E/I_M versus [SDS] plot from which the behavior of the polymer is then inferred. Yet it is interesting to note that these plots exhibit two main types of profiles. The first category of reported I_E/I_M versus [SDS] plots exhibits a behavior similar to the one shown in the inset of Figure 2 where the I_E/I_M ratio takes a small value at low SDS concentration, goes through a maximum at an SDS concentration close to the CMC, and decreases back to a low I_E/I_M ratio at high SDS concentration.³⁰ The second category of I_E/I_M versus [SDS] profiles exhibits a high I_E/I_M ratio at low SDS concentration, which drops down to a much lower value at high SDS concentration.^{28,29,31} The drop of the I_E/I_M ratio occurs often in the neighborhood of the CMC. These differences in the I_E/I_M versus [SDS] profiles are a consequence of differences in the level of pyrene labeling, the mode of binding of the surfactant onto the pyrene-labeled polymer, and the low quantum yield of pyrene aggregates.^{24,28,29} It is hoped that the present study, aimed at determining the fractions of all emissive pyrene species present in a Py-AP solution, will contribute in the future toward providing a better rational for explaining the I_E/I_M versus [SDS] profiles.

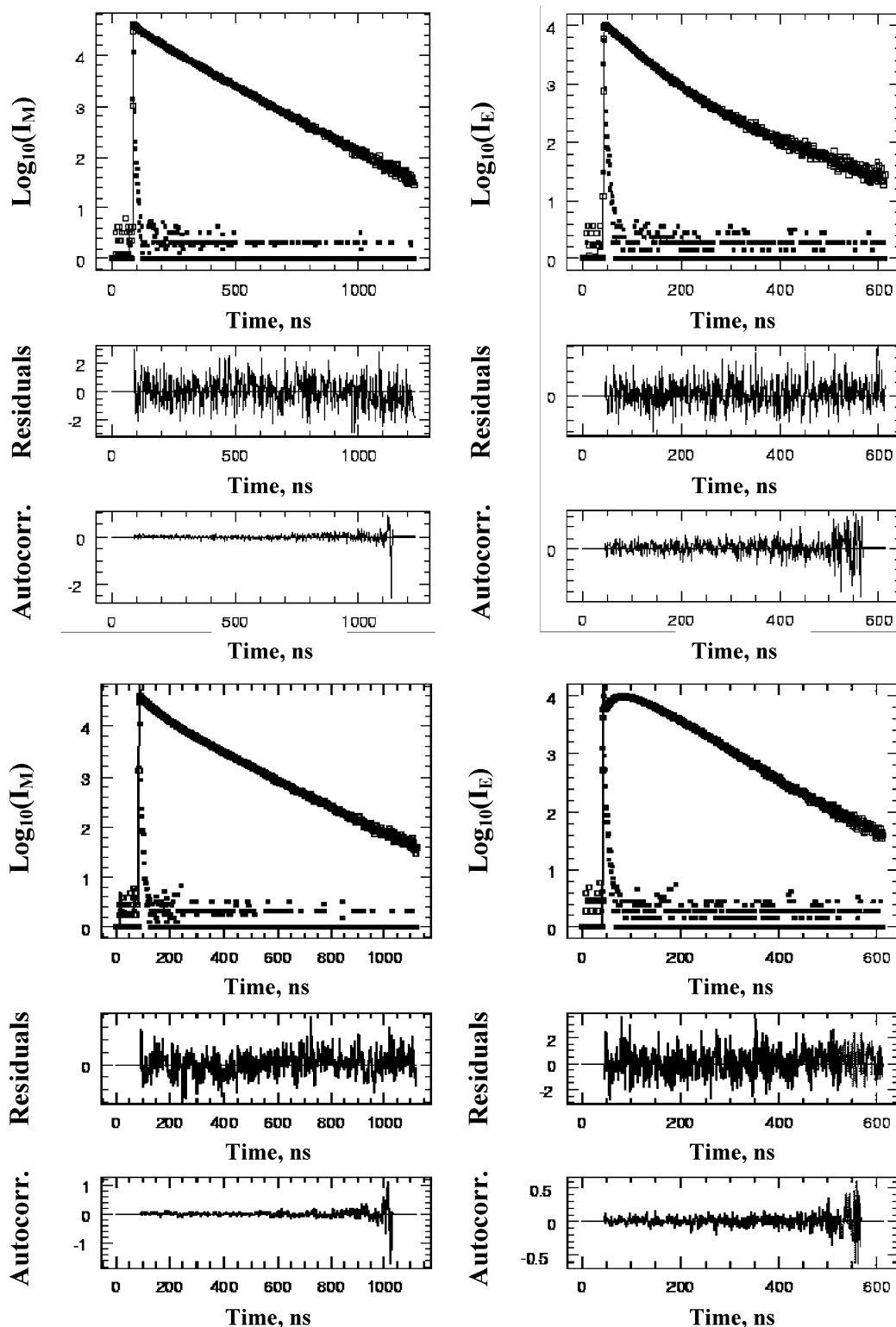


Figure 3. Monomer (left) and excimer (right) fluorescence decays of Py-HASE in 0.01 M Na_2CO_3 aqueous solution at pH 9 without SDS (top panel) and with 4.25×10^{-3} mol/L of SDS (bottom panel). The samples were excited at 344 nm. The monomer and excimer fluorescence decays were acquired at 375 and 510 nm, respectively. The decays were fitted globally by using sums of exponentials. The χ^2 were 1.13 and 1.09 for the top and bottom panels, respectively.

Beside the I_E/I_M ratio, the excimer fluorescence decays are also profoundly affected when SDS is added to a Py-HASE solution. At low SDS concentration, most pyrene groups are aggregated ($f_{\text{agg}} = 0.69$)¹³ and excimer formation occurs mostly inside a pyrene aggregate. Since the pyrene pendants are located close to one another inside an aggregate, excimer formation occurs on a fast time scale and hardly any rise time is observed in the excimer decay shown in Figure 3 (top panel). On the

other hand, a distinct rise time is observed for Py-HASE solutions containing 4.25×10^{-3} mol/L of SDS, as shown in Figure 3 (bottom panel). This is because the pyrene pendants are molecularly separated inside the SDS micelles and the formation of excimer is delayed by the time taken by two pyrene pendants to encounter.

The monomer and excimer fluorescence decays of Py-HASE obtained at several SDS concentrations were fitted globally with

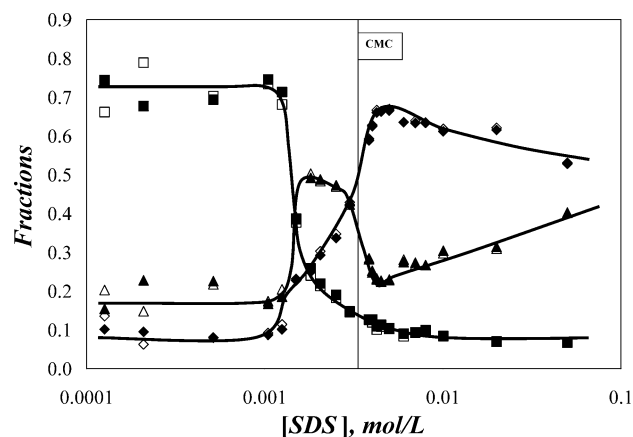


Figure 4. Fractions f_{diff} (\diamond and \blacklozenge), f_{free} (\triangle and \blacktriangle), and f_{agg} (\square and \blacksquare) as a function of SDS concentration. The hollow and filled symbols indicate that the analysis was performed with a sum of exponentials or the blob model, respectively.

eqs 12 and 13 assuming that the diffusional encounters between pyrene pendants were handled with the blob model (cf. eqs 7 and 9) or a sum of exponentials (cf. eqs 18 and 19). As described in the Theory section, the fluorescence decays of the pyrene monomer provide the “time-dependent rate constant” of excimer formation, $f(t)$, whereas the analysis of the rise time of the excimer decays yields information about the level of aggregation existing between pyrene pendants. The lifetime of the pyrene monomer, τ_M , was fixed in the analysis to equal 165 ns, which is a good estimate of the lifetime of the Py-PEO model compound in aqueous solution with (162 ns) or without (169 ns) SDS. When the global analysis was carried out by using the blob model equation to fit the monomer and excimer fluorescence decays, the parameters A_2 , A_3 , and A_4 were held the same in the expressions of $G_M(t)$ and $G_E(t)$ used in eqs 12 and 13, respectively. Similarly, the decay times τ_i and preexponential factors a_i were held the same in $G_M(t)$ and $G_E(t)$ for the global analysis of the monomer and excimer fluorescence decays with eqs 12 and 13, respectively, when using a sum of exponentials to model the dynamic encounters between the pyrene pendants. Only two exponentials were necessary for $G_M(t)$ and $G_E(t)$ in eqs 12 and 13, i.e., $n = 2$ in the series of eqs 18 and 19. On the other hand, expressions related to the concentrations of the various emissive pyrene species at equilibrium, namely, $[\text{Py}_{\text{diff}}^*]_{(t=0)}$, $[\text{Py}_{\text{free}}^*]_{(t=0)}$, $(\epsilon_{\text{E0}} k_{\text{rad}}^{\text{E0(agg)}} / \epsilon_M k_{\text{rad}}^{\text{E0(diff)}})[\text{E0}^*]_{(t=0)}$, and $(\epsilon_D k_{\text{rad}}^{\text{D}} / \epsilon_M k_{\text{rad}}^{\text{E0(diff)}})[\text{D}^*]_{(t=0)}$ (cf. Equations 12 and 13), were optimized separately in each equation.

The fits obtained from the global analysis of the monomer and excimer decays were very good with χ^2 ranging from 0.97 to 1.21 when a sum of exponentials was used to fit the monomer decays, or from 0.97 to 1.18 when using the blob model analysis. The residuals and the autocorrelation function of the residuals were always randomly distributed around zero, as can be seen in the typical examples shown in Figure 3. The fractions f_{diff} , f_{free} , f_{E0} , and f_{D} whose definition is given in eqs 14–17 were determined by both methods and compared. The results are shown in Figure 4. The parameters retrieved from the analyses are listed in Tables 2 and 3 in the Supporting Information.

The obvious result of Figure 4 is that both methods of analysis of the fluorescence decays yield quasi-identical profiles for the fractions f_{diff} , f_{free} , and f_{agg} ($f_{\text{agg}} = f_{\text{E0}} + f_{\text{D}}$), which establishes unambiguously that the determination of these fractions does not depend on the model chosen to describe the diffusional encounters between pyrene pendants. For SDS concentrations smaller than 1.25×10^{-3} mol/L, the fractions remain constant

and equal 0.10 ± 0.03 , 0.20 ± 0.03 , and 0.70 ± 0.05 for f_{diff} , f_{free} , and f_{agg} , respectively. For SDS concentrations larger than 1.25×10^{-3} mol/L, the pyrene aggregates are broken up and f_{agg} drops from 0.70 ± 0.05 down to a value of 0.08 ± 0.01 for SDS concentrations larger than 6.0×10^{-3} mol/L. An important parameter to know about this system is the CMC of SDS in the 0.01 M Na_2CO_3 aqueous solution at pH 9 solution. It was determined via surface tension measurements and found to equal 3.5×10^{-3} mol/L (cf. Supporting Information), substantially higher than the SDS concentration where the destruction of pyrene aggregates starts (1.25×10^{-3} mol/L). The fraction of pyrenes forming excimer by diffusion, f_{diff} , increases from a low value of 0.10 ± 0.03 up to a maximum of 0.66 at an SDS concentration of 4.5×10^{-3} mol/L, very close to the CMC. This effect results from having few SDS micelles into which the pyrene pendants are concentrated, favoring excimer formation via diffusion. The maximum of the f_{diff} versus [SDS] profile coincides with that of the I_E/I_M ratio observed for a SDS concentration of 4.55×10^{-3} mol/L. At higher SDS concentrations, f_{diff} decreases as more SDS micelles are formed and the pyrene pendants distribute themselves into more SDS micelles. Consequently less excimer forms by diffusion and the I_E/I_M ratio decreases (cf. inset in Figure 2). The fraction of isolated pyrenes, f_{free} , exhibits a rather interesting profile. At low SDS concentration ($< 1.25 \times 10^{-3}$ mol/L), it is constant and equals 0.20 ± 0.03 . At intermediate SDS concentrations between 1.25×10^{-3} (where f_{agg} plummets) and 6.0×10^{-3} mol/L (where f_{agg} reaches its low-value plateau), f_{free} passes through a maximum at 0.48 ± 0.01 between 1.8×10^{-3} and 2.5×10^{-3} mol/L. Because the ratio I_1/I_3 in this concentration range is similar to that of Py-PEO in 0.01 M Na_2CO_3 aqueous solution at pH 9, this result indicates that a large fraction of the pyrene pendants are released into the aqueous solution and are too far apart to form excimer by diffusion. Past the SDS concentration of 2.5×10^{-3} mol/L, f_{free} passes through a minimum of 0.22 for an SDS concentration of 4.5×10^{-3} mol/L, before showing a continuous increase as more SDS is added to the solution. In the concentration range between 2.5×10^{-3} and 4.5×10^{-3} mol/L, SDS micelles form and the pyrene pendants are being drawn into a few micelles where they can form excimer by diffusion. The fraction f_{diff} increases while f_{free} decreases. Past the CMC (3.5×10^{-3} mol/L), more micelles are formed and the pyrene pendants distribute themselves among many micelles increasing the probability of finding single pyrenes inside SDS micelles. This results in the continuous increase observed for f_{free} at higher SDS concentrations.

The f_{agg} versus [SDS] profile shown in Figure 4 provides qualitative support to the fact that pyrene aggregates exhibit a low fluorescence quantum yield. At low SDS concentration ([SDS] $< 1.25 \times 10^{-3}$ mol/L), the pyrene pendants are strongly associated and f_{agg} equals 0.70 ± 0.05 . Indeed out of all pyrenes forming an excimer, the fraction of pyrenes forming excimer by diffusion ($f_{\text{E(diff)}}$) given in Tables 2 and 3 of the Supporting Information equals only 0.14 ± 0.05 , suggesting strong association. It must be noted that under those conditions of strong association, f_{agg} is a reasonable estimate of the fraction of emissive pyrenes which are aggregated (cf. Appendix). Yet in this same range of SDS concentration, the ratio I_E/I_M shown in the inset of Figure 2 is small. If the quantum yield of an excimer formed either by diffusion ([SDS] $> 4.25 \times 10^{-3}$ mol/L) or by direct excitation of a pyrene aggregate ([SDS] $< 1.25 \times 10^{-3}$ mol/L) were the same, the I_E/I_M ratio would be expected to be large at low SDS concentration, since most pyrene pendants are associated and excimer formation is favored when

the pyrene pendants are close to one another. This is not observed. The only rational capable of explaining the opposite trends observed for the I_E/I_M ratio shown in the inset of Figure 2 and the f_{agg} profile shown in Figure 4 implies that the fluorescence quantum yield of the excimer formed from the direct excitation of ground-state pyrene aggregates is much lower than that of the excimer formed by the diffusional encounters between pyrene pendants. This observation agrees completely with earlier reports.^{24,28,29} According to this statement, the trend observed in the inset of Figure 2 can be described as follows. At low SDS concentration, the numerous pyrene aggregates emit little fluorescence and the I_E/I_M ratio is small. When the addition of SDS induces the melting of the pyrene aggregates, excimer formation occurs by diffusion. The fluorescence quantum yield of the excimer formed by diffusion is larger and the I_E/I_M ratio increases. The I_E/I_M ratio keeps on increasing until the number of SDS micelles present in the solution is so large that the pyrene pendants are distributed into separate micelles, which hinders the process of excimer formation by diffusion. This induces the decrease observed for the I_E/I_M ratio in the inset of Figure 2 at high SDS concentration.

The data shown in Figure 4 demonstrate that both analyses retrieve the same f_{diff} , f_{free} , f_{E0} , and f_D fractions. To confirm that the two analyses are equivalent, the behavior of the “time-dependent rate constant” of excimer formation obtained by both analyses should be compared. To do so, the average rate constant of excimer formation by diffusion ($\langle k_{diff} \rangle$) was determined for both methods by using a slightly modified method of an earlier publication.^{17a} When the blob model equation is used, $\langle k_{diff} \rangle$ is given by eq 20.

$$\langle k_{diff} \rangle = \left[\int_{t=0}^{\infty} \frac{[Py_{diff}^*]_{(t)}}{[Py_{diff}^*]_{(t=0)}} dt \right]^{-1} - \frac{1}{\tau_M} = \left[\int_{t=0}^{\infty} \exp(-A_2 + \frac{1}{\tau_M} t - A_3(1 - \exp(-A_4 t)) dt \right]^{-1} - \frac{1}{\tau_M} \quad (20)$$

When using sums of exponentials to fit the fluorescence decays of the pyrene monomer, $\langle k_{diff} \rangle$ is given by eq 21.

$$\langle k_{diff} \rangle = \left[\int_{t=0}^{\infty} \frac{[Py_{diff}^*]_{(t)}}{[Py_{diff}^*]_{(t=0)}} dt \right]^{-1} - \frac{1}{\tau_M} = \left[\int_{t=0}^{\infty} \frac{\sum_{i=1}^n a_i e^{-t/\tau_i}}{\sum_{i=1}^n a_i} dt \right]^{-1} - \frac{1}{\tau_M} = \left[\frac{\sum_{i=1}^n a_i \tau_i}{\sum_{i=1}^n a_i} \right]^{-1} - \frac{1}{\tau_M} \quad (21)$$

The result of these operations is shown in Figure 5.

Here again, a perfect agreement is obtained between the two analyses. Within experimental error, $\langle k_{diff} \rangle$ remains constant and equal to $1.0 \pm 0.3 \times 10^7 \text{ s}^{-1}$ for SDS concentrations lower than $2.0 \times 10^{-3} \text{ mol/L}$. $\langle k_{diff} \rangle$ then increases and passes through a maximum of $2.7 \times 10^7 \text{ s}^{-1}$ for an SDS concentration of $3.0 \times 10^{-3} \text{ mol/L}$, before decreasing to a plateau value of $1.0 \pm 0.1 \times 10^7 \text{ s}^{-1}$ for SDS concentrations larger than $10.0 \times 10^{-3} \text{ mol/L}$. Interestingly, $\langle k_{diff} \rangle$ takes its maximum value at a SDS concentration that is close to the CMC ($3.5 \times 10^{-3} \text{ mol/L}$). The inset in Figure 2 indicates that the I_E/I_M ratio shows its

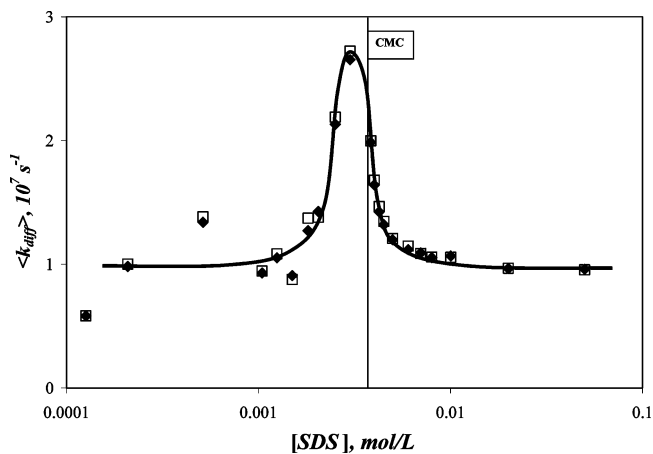


Figure 5. Average rate constant of excimer formation by diffusion, $\langle k_{diff} \rangle$, obtained from the global analysis of the monomer and excimer decays by using a sum of exponentials (\square) or the blob model analysis (\blacklozenge).

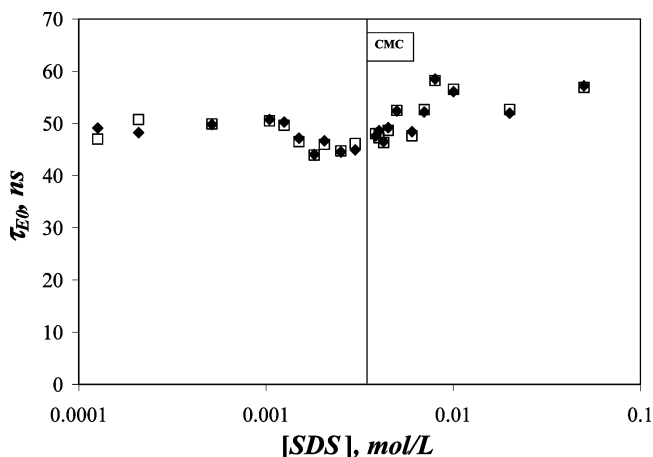


Figure 6. Excimer lifetime, τ_{E0} , obtained from the global analysis of the monomer and excimer decays by using a sum of exponentials (\square) or the blob model analysis (\blacklozenge).

steepest increase at an SDS concentration of $3.0 \times 10^{-3} \text{ mol/L}$, where $\langle k_{diff} \rangle$ takes its maximum value. It seems that the pyrene pendants forming excimer via diffusion are concentrated in a few hydrophobic aggregates just before the CMC of SDS, yielding a large rate constant of excimer formation by diffusion. These results suggest that the efficiency of the process of excimer formation (given by the I_E/I_M ratio) is a combination of the fraction of pyrene monomers forming excimer by diffusion (f_{diff}) and the rate of excimer formation by diffusion ($\langle k_{diff} \rangle$).

The last parameter to be considered when comparing the results obtained by both methods is the excimer lifetime, τ_{E0} . It is plotted as a function of SDS concentration in Figure 6. Within experimental error, τ_{E0} is found to remain constant with SDS concentration. It equals $49 \pm 4 \text{ ns}$, which is a reasonable value. It agrees with the τ_{E0} values of 51 ± 2 , 53 ± 3 , and 50 ns obtained for Py-HASE,⁹ pyrene-labeled poly(*N,N*-dimethyl acrylamide),¹⁰ and a pyrene-labeled poly(acrylic acid) in aqueous solutions,²² respectively. More importantly, the τ_{E0} versus [SDS] profiles shown in Figure 6 are indistinguishable demonstrating that both analyses yield identical τ_{E0} values.

At this stage, it has been shown that both analyses yield identical fractions f_{diff} , f_{free} , and f_{agg} for an aqueous Py-HASE solution (cf. Figure 4), identical average rate constants of excimer formation by diffusion ($\langle k_{diff} \rangle$ in Figure 5), and identical excimer lifetimes (τ_{E0} in Figure 6). Of particular interest to the

study of APs, the parameter f_{agg} can be determined quantitatively and it represents a close estimate of the fraction of emissive species of aggregated pyrenes at low ($<1.25 \times 10^{-3}$ mol/L, high level of pyrene aggregation) and high ($>4.25 \times 10^{-3}$ mol/L, low level of pyrene aggregation) SDS concentration, since under these conditions, a close equivalence is expected between f_{diff} , f_{free} , f_{E} , and f_{D} and the corresponding fractions of emissive pyrene species (cf. discussion in the Appendix).

Since the *blob* model equation is a stretched exponential, i.e., an infinite sum of exponentials, it is satisfying to observe that analyses of the fluorescence decays with the *blob* model and a finite sum of exponentials yield similar trends. Yet not all sums of exponentials can be fitted with a stretched exponential of the *blob* model type. This is illustrated in Figure 7 where monomer and excimer decays simulated with eqs 22 and 23 were fitted with eqs 12 and 13, respectively, using the expressions of $G_{\text{M}}(t)$ and $G_{\text{E}}(t)$ obtained by modeling the diffusional encounters between pyrene pendants with either the *blob* model or a sum of exponentials.

$$I_{\text{M}}(t) = 0.333e^{-t/10\text{ns}} + 0.333e^{-t/40\text{ns}} + 0.333e^{-t/100\text{ns}} + 0.050e^{-t/165\text{ns}} \quad (22)$$

$$I_{\text{E}}(t) = -0.393e^{-t/10\text{ns}} - 1.373e^{-t/40\text{ns}} + 0.126e^{-t/100\text{ns}} + 1.695e^{-t/49\text{ns}} + 0.055e^{-t/150\text{ns}} \quad (23)$$

In eqs 22 and 23, the lifetimes τ_{M} , τ_{E0} , and τ_{D} were chosen to equal 165, 49, and 150 ns, respectively. The preexponential factors in eqs 22 and 23 were chosen so that f_{diff} , f_{free} , f_{E0} , and f_{D} would equal 0.86, 0.04, 0.05, and 0.05, respectively. The preexponential factors in eq 23 were obtained by assuming that $\epsilon_{\text{E0}} = \epsilon_{\text{D}} = \epsilon_{\text{M}}$ and $k_{\text{rad}}^{\text{E0(agg)}} = k_{\text{rad}}^{\text{D}} = k_{\text{rad}}^{\text{E0(diff)}}$ in eq 13. Fluorescence decays of the monomer and excimer were simulated with 100,000 counts at the decay maximum and added Poisson noise according to established procedures.³² From the residuals shown in the bottom panel of Figure 7, it is clear that the analysis of the fluorescence decays with the *blob* model cannot handle eqs 22 and 23. This study demonstrates that the procedure using a sum of exponentials to model the diffusional encounters between pyrenes is more general than the *blob* model-based procedure.

Conclusions

The associations taking place between the pyrene pendants of a Py-HASE were monitored as a function of the concentration of surfactant added to the solution. Two analysis methods were applied. The first one used a *blob* model to describe the diffusional encounters between the pyrene pendants. The second one made no assumption on how excimers form via diffusion so that the fluorescence decays of the pyrene monomer and excimer could be fitted by sums of exponentials. For both procedures, the monomer and excimer decays were fitted globally to ensure higher accuracy of the retrieved parameters. The fits carried out with both procedures yielded identical results in terms of fractions f_{diff} , f_{free} , f_{E0} , and f_{D} as defined in eqs 14–17, rate of excimer formation, and excimer lifetime. This study demonstrates that both analyses are equivalent and that the determination of the fractions f_{diff} , f_{free} , f_{E0} , and f_{D} does not require an exact physical understanding of how excimer formation by diffusion occurs. The widespread use of sums of exponentials to analyze fluorescence decays should make the

proposed analysis more appealing to the scientific community than the earlier procedure based on the *blob* model.

Appendix

One disadvantage of time-resolved fluorescence experiments is that no direct relationship exists between the fluorescence signals of a mixture of emitters and the concentrations of the emitters. This is because the fluorescence intensity depends on the concentration, the extinction coefficient, and the rate constant of emission of the chromophores, as illustrated in eqs 12 and 13. Consequently difficulties arise for interpreting fluorescence data when several chromophores are present simultaneously in the solution, as is the case for many pyrene-labeled polymers. Yet it is argued in the following discussion that conditions can be defined where an equivalence exists between the f_{diff} , f_{free} , f_{E0} , and f_{D} fractions obtained by fluorescence (cf. eqs 14–17) and the fractions of the concentrations of the corresponding emissive pyrene species. To do so, all pyrene species assumed to be present in solution are described and the relative value of their radiative rate constant and extinction coefficient is considered.

Since a pyrene monomer is the same whether it is isolated (Py_{free}) or about to form an excimer via diffusion (Py_{diff}), both species experiencing the same environment have the same extinction coefficient (ϵ_{M}) and radiative rate constant ($k_{\text{rad}}^{\text{M}}$) in eq 12. However, ϵ_{M} and $k_{\text{rad}}^{\text{M}}$ are bound to take different values when pyrene experiences different environments. Consequently, ϵ_{M} and $k_{\text{rad}}^{\text{M}}$ can be assumed to be constant under conditions where a majority of pyrene monomers are in a similar environment. However, the values of ϵ_{M} and $k_{\text{rad}}^{\text{M}}$ will be affected by a transition during which the polarity of the environment experienced by the pyrene monomers is altered, i.e., when at least two substantial fractions of the pyrene monomers are present at the same time in two different environments. Nevertheless, under homogeneous conditions away from a transition, ϵ_{M} and $k_{\text{rad}}^{\text{M}}$ will take well-defined values.

The pyrene species yielding an excimer or an excimer-like emission are more complicated to handle. First of all, the absorption spectrum of a pyrene-labeled polymer is distorted when pyrene aggregates are present.⁶ Consequently the extinction coefficients ϵ_{E0} and ϵ_{D} are expected to be different and certainly lower than ϵ_{M} . Yet since ϵ_{E0} and ϵ_{D} are the extinction coefficients of pyrene aggregates, they should take similar values (i.e. $\epsilon_{\text{E0}} \approx \epsilon_{\text{D}}$). Second, several reports have raised suspicion that pyrene aggregates in water would have a lower quantum yield possibly due to pyrene self-quenching inside an aggregate.^{24,28,29} Consequently the rate constant $k_{\text{rad}}^{\text{E0(diff)}}$ might be different from $k_{\text{rad}}^{\text{E0(agg)}}$ and $k_{\text{rad}}^{\text{D}}$.

In the case of the radiative rate constants, it can certainly be argued that $k_{\text{rad}}^{\text{E0(agg)}}$ and $k_{\text{rad}}^{\text{D}}$ take similar values, since they both describe the emission of pyrene aggregates. Furthermore, $k_{\text{rad}}^{\text{E0(diff)}}$ is expected to be equal to $k_{\text{rad}}^{\text{E0(agg)}}$ when an excimer is formed from the diffusional encounters between an excited pyrene monomer and a pyrene aggregate since the emitting species that results from the encounter is an excited pyrene aggregate. This latter case is encountered when dealing with a pyrene-labeled polymer whose pyrene pendants are strongly aggregated. Under conditions where the pyrene pendants are hardly aggregated, the pyrene aggregates are sparse and made of a few pyrenes and they cannot be subject to self-quenching. Consequently, $k_{\text{rad}}^{\text{E0(agg)}}$, $k_{\text{rad}}^{\text{D}}$, and $k_{\text{rad}}^{\text{E0(diff)}}$ should adopt a value comparable to that of the excimer, $k_{\text{rad}}^{\text{E0}}$. Thus the radiative rate constants $k_{\text{rad}}^{\text{E0(agg)}}$, $k_{\text{rad}}^{\text{D}}$, and $k_{\text{rad}}^{\text{E0(diff)}}$ should take values similar to

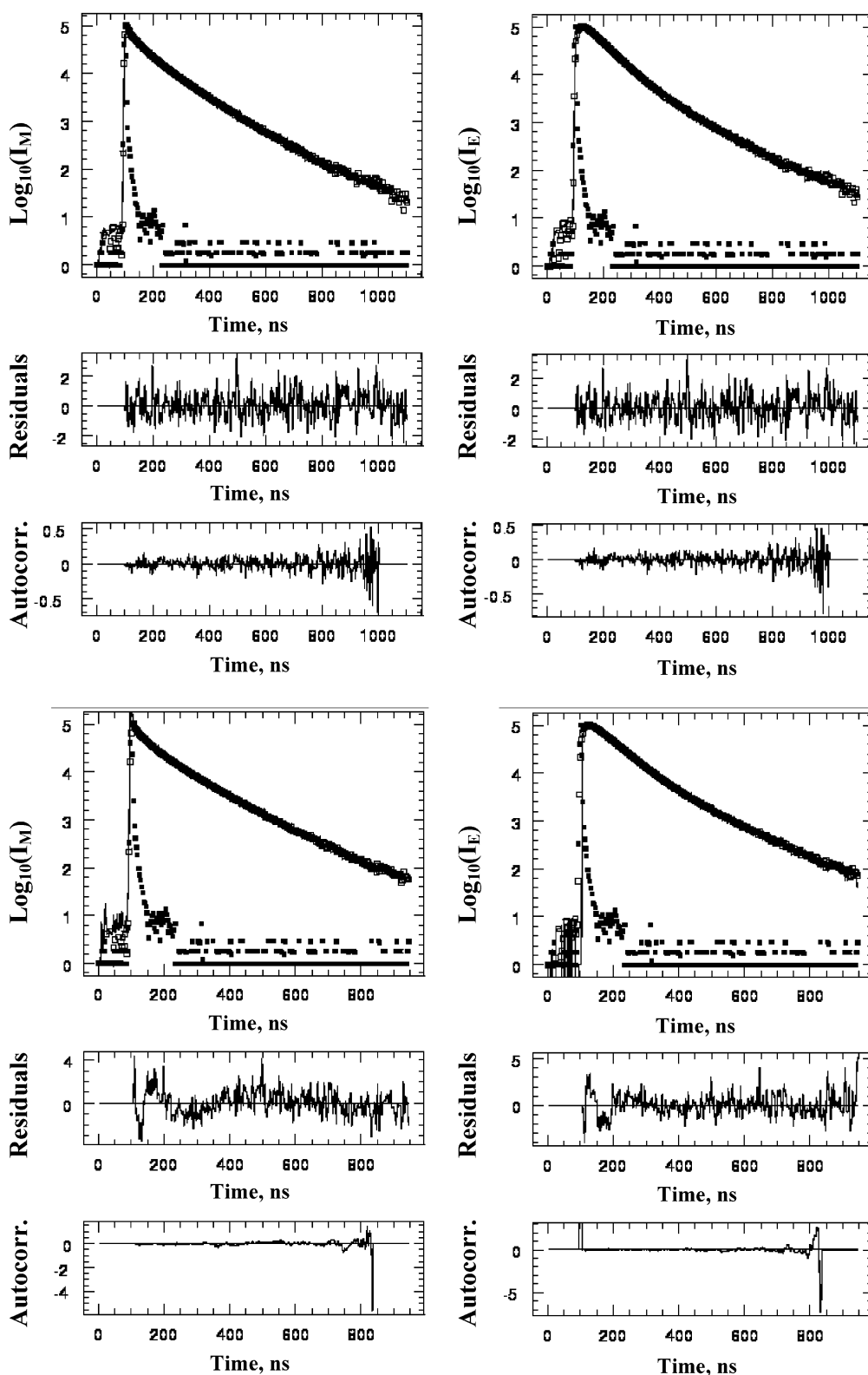


Figure 7. Results of the analysis with eqs 12 and 13 of the monomer and excimer fluorescence decays simulated with eqs 22 and 23 assuming that excimer formation by diffusion can be modeled by a sum of exponentials (top panel) or the *blob* model (bottom panel). The χ^2 values equalled 1.02 and 1.68 for the top and bottom panel, respectively.

$k_{\text{rad}}^{\text{E0(agg)}}$ or $k_{\text{rad}}^{\text{E0}}$ under conditions where the pyrenes exhibit strong or weak associations, respectively. Due to self-quenching, $k_{\text{rad}}^{\text{E0(agg)}}$ is expected to be small when the pyrene pendants aggregate strongly whereas $k_{\text{rad}}^{\text{E0}}$ is expected to be large when little pyrene aggregation is occurring.

Although the extinction coefficients ϵ_{E0} and ϵ_{D} should be smaller than ϵ_{M} , the difference should not be drastic. In the case

of DNA base pairs, melting of some DNA helices has been shown to result in a 34% reduction of the absorbance (i.e. hypochromism).³³ In the case of Py-HASE, a forthcoming publication will present an analysis leading to the conclusion that ϵ_{E0} (assuming that $\epsilon_{\text{D}} \approx \epsilon_{\text{E0}}$) is 25% smaller than ϵ_{M} . Because ϵ_{E0} and ϵ_{D} are similar and take a value close to ϵ_{M} and because $k_{\text{rad}}^{\text{E0(agg)}}$ and $k_{\text{rad}}^{\text{D}}$ are close and take values similar to

$k_{\text{rad}}^{\text{E0(diff)}}$ when the pyrene pendants are strongly or weakly associated, under these conditions, the fractions f_{diff} , f_{free} , f_{E0} , and f_{D} represent a reasonable estimate of the fractions of all emissive pyrene species present in solution (cf. eqs 14–17). At the transition where the pyrene aggregates melt, f_{diff} , f_{free} , f_{E0} , and f_{D} provide information on how the fractions of all the emissive pyrene species present in solution behave.

Supporting Information Available: Diagram of surface tension measurements of SDS solutions in 0.01 M Na_2CO_3 at pH 9; tables of $G_{\text{M}}(t)$ and $G_{\text{E}}(t)$, as well as parameters retrieved from the global analysis of the monomer and excimer fluorescence decays. This material is available free of charge via the Internet at <http://pubs.acs.org>.

References and Notes

- Olesen, K. R.; Bassett, D. R.; Wilkerson, C. L. *Prog. Org. Coat.* **1998**, *35*, 161–170.
- Jenkins, R. D.; DeLong, L. M.; Bassett, D. R. *Hydrophilic Polymers. Performance with Environmental Acceptability*; Advances in Chemistry Series No. 248; American Chemical Society: Washington, DC, 1996; pp 425–447. Hansson, P.; Lindman, B. *Curr. Opin. Colloid Interface Sci.* **1996**, *1*, 604–613. Winnik, M. A.; Yekta, A. *Curr. Opin. Colloid Interface Sci.* **1997**, *2*, 424–436. Iliopoulos, I. *Curr. Opin. Colloid Interface Sci.* **1998**, *3*, 493–498.
- Annabale, T.; Buscall, R.; Ettelaie, R.; Whittlestone, D. *J. Rheol.* **1993**, *37*, 695–726. Volpert, E.; Selb, J.; Candau, F. *Macromolecules* **1996**, *29*, 1452–1463. Tirtaatmadja, V.; Tam, K. C.; Jenkins, R. D. *Macromolecules* **1997**, *30*, 3271–3282.
- Noda, T.; Hashidzume, A.; Morishima, Y. *Macromolecules* **2001**, *34*, 1308–1317. Morishima, Y.; Nomura, S.; Ikeda, T.; Seki, M.; Kamachi, M. *Macromolecules* **1995**, *28*, 2874–2881.
- Morawetz, H. *J. Polym. Sci. A: Polym. Chem.* **1999**, *37*, 1725–1735. Morawetz, H. *J. Lumin.* **1989**, *43*, 59–71. Yekta, A.; Winnik, M. A. *NATO ASI Ser., Ser. E* **1996**, *327*, 433–455. Winnik, F. M.; Regismond, S. T. A. *Colloids Surf. A* **1996**, *118*, 1–39.
- Winnik, F. M. *Chem. Rev.* **1993**, *93*, 587–614.
- Richey, B.; Kirk, A. B.; Eisenhart, E. K.; Fitzwater, S.; Hook, J. J. *Coat. Technol.* **1991**, *63*, 31–40.
- Leibler, L.; Rubinstein, M.; Colby, R. H. *Macromolecules* **1991**, *24*, 4701–4707. Annable, T.; Buscall, R.; Ettelaie, R.; Whittlestone, D. *J. Rheol.* **1993**, *37*, 695–726.
- Prazeres, T. J. V.; Beingessner, R.; Duhamel, J.; Olesen, K.; Shay, G.; Bassett, D. R. *Macromolecules* **2001**, *34*, 7876–7884.
- Kanagalingam, S.; Ngan, C. F.; Duhamel, J. *Macromolecules* **2002**, *35*, 8560–8570.
- Duhamel, J.; Kanagalingam, S.; O'Brien, T.; Ingratta, M. *J. Am. Chem. Soc.* **2003**, *125*, 12810–12822.
- Zhang, M.; Duhamel, J.; van Duin, M.; Meessen, P. *Macromolecules* **2004**, *37*, 1877–1890.
- Siu, H.; Duhamel, J. *Macromolecules* **2004**, *37*, 9287–9289.
- Birks, J. B. *Photophysics of Aromatic Molecules*; Wiley: New York, 1970; p 351.
- Winnik, M. A. *Acc. Chem. Res.* **1985**, *18*, 73–79.
- Lee, S.; Winnik, M. A. *Macromolecules* **1997**, *30*, 2633–2641.
- (a) Winnik, M. A.; Egan, L. S.; Tencer, M.; Croucher, M. D. *Polymer* **1987**, *28*, 1553–1560. (b) Winnik, M. A.; Li, X.-B.; Guillet, J. E. *Macromolecules* **1984**, *17*, 699–702.
- Mathew, A. K.; Siu, H.; Duhamel, J. *Macromolecules* **1999**, *32*, 7100–7108.
- Kanagalingam, S.; Spartalis, J.; Cao, T.-M.; Duhamel, J. *Macromolecules* **2002**, *35*, 8571–8577.
- Picarra, S.; Relogio, P.; Afonso, C. A. M.; Martinho, J. M. G.; Farinha, J. P. S. *Macromolecules* **2004**, *37*, 1670–1670. Picarra, S.; Relogio, P.; Afonso, C. A. M.; Martinho, J. M. G.; Farinha, J. P. S. *Macromolecules* **2003**, *36*, 8119–8129.
- Picarra, S.; Duhamel, J.; Fedorov, A.; Martinho, J. M. G. *J. Phys. Chem. B* **2004**, *108*, 12009–12015.
- Seixas de Melo, J.; Costa, T.; Miguel, M. d. G.; Lindman, B.; Schillen, K.; *J. Phys. Chem. B* **2003**, *107*, 12605–12621.
- Turro, N. J.; Arora, K. S. *Polymer* **1986**, *27*, 783–796. Ringsdorf, H.; Venzmer, J.; Winnik, F. M. *Macromolecules* **1991**, *24*, 1678–1686. Winnik, F. M.; Winnik, M. A.; Tazuke, S.; Ober, C. K. *Macromolecules* **1987**, *20*, 38–44. Morishima, Y.; Mizusaki, M.; Yoshida, K.; Dubin, P. L. *Colloids Surf. A* **1999**, *147*, 149–159. Mizusaki, M.; Morishima, Y.; Dubin, P. L. *J. Phys. Chem. B* **1998**, *102*, 1908–1915.
- Anghel, D. F.; Alderson, V.; Winnik, F. M.; Mizusaki, M.; Morishima, Y. *Polymer* **1998**, *39*, 3035–3044.
- Jansens, L. D.; Boens, N.; Ameloot, M.; De Schryver, F. C. *J. Phys. Chem.* **1990**, *94*, 3564–3576. Gehlen, M. H.; De Schryver, F. C. *Chem. Rev.* **1993**, *93*, 199–221.
- Seng, W. P.; Tam, K. C.; Jenkins, R. D.; Bassett, D. R. *Langmuir* **2000**, *16*, 2151–2156.
- Seng, W. P.; Tam, K. C.; Jenkins, R. D.; Bassett, D. R. *Macromolecules* **2000**, *33*, 1727–1733.
- Anghel, D. F.; Toca-Herrera, J. L.; Winnik, F. M.; Rettig, W.; v. Kliting, R. *Langmuir* **2002**, *18*, 5600–5606.
- Winnik, F. M.; Regismond, S. T. A.; Goddard, E. D. *Langmuir* **1997**, *13*, 111–114.
- Quina, F.; Abuin, E.; Lissi, E. *Macromolecules* **1990**, *23*, 5173–5175. Maltesh, C.; Somasundaran, P. *Langmuir* **1992**, *8*, 1926–1930. Hu, Y.-Z.; Zhao, C.-L.; Winnik, M. A.; Sundararajan, P. R. *Langmuir* **1990**, *6*, 880–883.
- Winnik, F. M.; Ringsdorf, H.; Venzmer, J. *Langmuir* **1991**, *7*, 912–917. Winnik, M. A.; Bystryak, S. M.; Siddiqui, J. *Macromolecules* **1999**, *32*, 624–632. Winnik, F. M.; Winnik, M. A.; Tazuke, S. *J. Phys. Chem.* **1987**, *91*, 594–597.
- Duhamel, J.; Yekta, A.; Ni, S.; Khaykin, Y.; Winnik, M. A. *Macromolecules* **1993**, *26*, 7024–7030.
- Voet, D.; Gratzer, W. B.; Cox, R. A.; Doty, P. *Biopolymers* **1963**, *1*, 193–208.